HOVERING ROTOR PERFORMANCES: A PANEL METHOD COUPLED WITH A NAVIER-STOKES METHOD

J. Haertig - P. Gnemmi - Ch. Johé

French-German Research Institute of Saint-Louis
5 rue du Général-Cassagnou
68301 SAINT LOUIS CEDEX (France)

Abstract

The French-German Research Institute of Saint-Louis (ISL) is involved in aerodynamic research in order to predict the performances of hovering rotors.

An original approach is proposed to deal with this challenge: a full potential computation (PARSEC) is coupled with a Navier-Stokes computation (TASCflow). The full potential computation is used to predict the wake of the multi-bladed rotor and its aerodynamic coefficients. It also provides necessary boundary conditions on the nodes of the small volume surrounding one blade for Navier-Stokes computations.

Before applying this method to a new design of blades it is reasonable to examine the accuracy of this approach for classical rotor blades. Visualization of the tip vortex path and measurements of aerodynamic coefficients are carried out on the ISL rotor model (NACA0012 rectangular twisted blade) for many rotation speeds and blade tip incidence angles.

PARSEC and TASCflow numerical results are compared with experimental ones obtained on this rotor model. A good agreement on rotor performances is found, so that new blade designs can be studied in the future with this method.

1 - Introduction

The prediction of the 3D flow field of a hovering rotor is still a challenge. Owing to the lack of forced convection, the wake interacts strongly with blades, so that performances depend on the accuracy of the wake calculation.

An original approach consists in coupling a full potential computation with a Navier-Stokes one in order to solve this kind of problem on a workstation in an acceptable duration.

The potential equation of perfect inviscid fluid is solved by using a panel or a boundary element method. The theoretical background is briefly given, the wake model and the relaxation scheme used to reach the final equilibrium are also described in this paper.

The boundary conditions for the Navier-Stokes computation are calculated on a "small domain" surrounding one blade by using the results of the potential code PARSEC[1]. This procedure avoids the wake diffusion due to the Navier-Stokes computation and enables the use of a standard workstation to perform predictions.
The governing equations solved by the TASCflow[2] commercial code are the Reynolds-stress averaged Navier-Stokes equations recalled in the following.

ISL has built a rotor model operating in the open air and simulating the hovering flight, in order to study aerodynamic and aeroacoustic phenomena. This rotor model is able to reach transonic speed at the blade tip with a Reynolds number not too different from that of full-scale rotors. This equipment is briefly presented in this paper.

Computed results are compared with experimental ones (tip vortex path, thrust and torque coefficients) obtained on the ISL rotor model.

2 - Theory

2.1 - Field Panel Method (PARSEC)

2.1.1 - Background

Let us consider an isolated hovering rotor, rotating around a vertical axis at the angular velocity Ω, and assuming a potential flow; the velocity at any $\vec{x}$ point is given by:

$$\vec{V}(\vec{x}) = \vec{\nabla}\vec{\varphi}\,, \qquad (1)$$

---

[1] **PARSEC**: Panneaux pour l'Aéroacoustique des Rotors avec Sillage à l'Equilibre, en Compressible, ISL.

[2] **TASCflow**: Advanced Scientific Computing Ltd., Waterloo, Ontario, Canada.

where φ is the solution of the full potential equation. Farassat's integral equation is used for the potential [1], it is completed with a field term, E_3, which represents nonlinearities in the flow [2, 3]:

$$4\pi\varphi(\vec{x}) = \iint_S \left[\frac{E_1}{r(1-M_r)}\right]_\tau dS + \iint_S \left[\frac{\varphi E_2}{r^2(1-M_r)}\right]_\tau dS + \iiint_V \left[\frac{E_3}{r(1-M_r)}\right]_\tau dV. \quad (2)$$

This E_3 term is only significant in a small volume around the blade tip. In this equation S represents the blade and the wake surfaces and V denotes the volume around the blade tip where the nonlinear terms cannot be neglected. r denotes the distance between the source element dS or dV and the point $\vec{x}$, M_r is the Mach number of the source element in the direction of the point $\vec{x}$ and τ indicates the emission time.

The compressibility can be neglected for the test cases presented in this paper. So the volume integral is left out and a classical "panel method" is used. In such a method, the potential is given by:

$$4\pi\varphi(\vec{x}) = \iint_{Sb} \mu_b \, \vec{n} \, \vec{\nabla}\left(\frac{1}{r}\right) dS + \iint_{Sw} \mu_W \, \vec{n} \, \vec{\nabla}\left(\frac{1}{r}\right) dS + \iint_{Sb} \frac{v_n}{r} dS. \quad (3)$$

$v_n = \vec{n}\,\vec{V}_b$, where $\vec{V}_b$ is the local velocity of the blade source element.

The normal velocity on the wake is continuous and only dipoles are distributed on it. At a given spanwise location, the dipole μ_W shed over the wake is given by:

$$\mu_W = \mu_{bu} - \mu_{bl}, \quad (4)$$

where μ_{bu} and μ_{bl} are dipole strengths on the upper and lower trailing edges of the blade, respectively. The Bernoulli equation yields:

$$\frac{d\mu_W}{dt} = 0. \quad (5)$$

Equations (3), (4) and (5) lead to the rotor flow once the wake surface is known and equation (1) enables the wake calculation.

A problem arises in such a computation when the shed wake vortices are cut by blades. In the case of hovering rotors, it happens near the blade root where the inner wake is moving up and near the blade tip at low thrust. The authors strongly reduce the circulation of the inner vortex to avoid this problem [4].

This method is acceptable in hover flight cases, but it is not satisfactory in advancing flight during which blade vortex interaction occurs. A PARSEC "partial panel removal" routine checks if any wake panel is cut by a blade: in that case, the influence of the panel surface is reduced.

Numerical tests of 2 airfoils in tandem where the downstream airfoil intersects the wake of the upstream one have been performed by using PARSEC and TASCflow. They have shown the efficiency of the method. Moreover, it has been found that the "partial panel removal" gives results quite similar to those obtained with the drastic inner vortex reduction, except very near the blade root.

2.1.2 - Viscous effects

An analytic skin friction law is used to take into account viscous effects in the boundary layer. This law assumes a turbulent boundary layer and is obtained by best fitting of data [5]. The friction coefficient used for taking into account viscous effects on a local blade section at a given incidence is expressed as follows:

$$Cf = Cf_0 + 7.5 \cdot 10^{-3} \, Cz^2, \quad (6)$$

where Cf_0 denotes the friction coefficient of a blade section at zero lift and Cz is the calculated lift coefficient of the blade section. Cf_0 is given by:

$$Cf_0 = \frac{3.2 \cdot 10^{-2}}{Re^{0.145}}\left(1 + 0.2\,M^2\right) \times \left(0.4678\,M^3 - 6.05 \cdot 10^{-2} M^2 - 5.1 \cdot 10^{-3} M + 1.0695\right). \quad (7)$$

Re and M are respectively the Reynolds and the Mach numbers determined for the local blade section. These two quantities are only used in the friction coefficient calculation.

2.1.3 - Wake model and discretization

At the beginning of the computation, a prescribed wake is used which will be deformed during the iteration process. This "near" wake is extended until downstream infinity by a "far" wake that is a semi-infinite solenoid. The blades and near wakes are meshed by Nb and Nw quadrilateral or triangular plane panels, where sources (v_n) and dipoles (μ) have a constant value.

A set of meridional planes with an azimuth angle ψ_i is chosen. At iteration n the intersections of the streamline, emanating from each trailing edge node, with ψ_i planes build the wake mesh $\vec{x}(n,i)$.

Equation (3) produces a system of Nb linear equations in which panels and far-wake influence coefficients have

analytic expressions [6, 7] and which determines the dipole distribution on blades and wakes. In the rotating frame, the discretized form of (1) gives the velocity at any $\vec{x}$ point:

$$\vec{V}(\vec{x}) = -\vec{\Omega} \times \vec{x} + \sum_{i=1}^{Nb} \nu_n(i) \vec{V}_S(\vec{x},i) + \sum_{i=1}^{Nb+Nw} \mu(i) \vec{V}_D(\vec{x},i) + \vec{V}_{Sol}(\vec{x}). \quad (8)$$

$\vec{V}_S(\vec{x},i)$ and $\vec{V}_D(\vec{x},i)$ are the induced velocities at $\vec{x}$ by a unit source and a unit dipole on an i panel and $\vec{V}_{Sol}(\vec{x})$ is the induced velocity by the far wake, all terms used in the code having analytic expressions [6, 7]. $\vec{V}_D(\vec{x},i)$ equals the induced velocity by the edge segments of the i panel with a unit circulation. It is calculated by using the Biot & Savart law showing a singular behaviour when the point $\vec{x}$ is close to a panel edge, a case which happens during the rolling-up of the vortex sheet.

An artificial "viscous core radius" is often used to bound $\vec{V}_D(\vec{x},i)$ but the velocity field and the whole flow depend on the value of this radius. This is not the case in the PARSEC code because the computation is founded on the "accumulation of displacements" of the panel corners.

2.1.4 - Wake relaxation scheme: accumulation of displacements

The wake surface consists of streamlines (vortex lines) emanating from the blade trailing edge. The 3D extension of the "flexible chain model" [7] leads to the downstream accumulation of the displacement of nodes and yields:

$$\vec{x}(n+1,i+1) - \vec{x}(n+1,i) = C\left(\vec{D}(n,i+1) + \vec{D}(n,i)\right). \quad (9)$$

Equation (9) expresses that the streamline segment i, $i+1$, at iteration $n+1$, is parallel to the mean displacement of corners i, $i+1$, at iteration n. The displacement $\vec{D}(n,i)$ (the time integral of the velocity at $\vec{x}(n,i)$) is always bounded without any "vortex core". The C constant is defined by writing that $\vec{x}(n,i)$ are in the meridional plane ψ_i, for all n and i. A prediction correction scheme is added in order to increase stability and convergence.

This is the key of the relaxation scheme adopted in the PARSEC code which runs on an IBM RS/6000 workstation and exhibits fast convergence.

The input files giving the geometry of the blades, collective pitch, coning angle and tip velocity have been adapted for each case presented below, but it must be pointed out that neither the prescribed initial helicoidal wake shape nor the code were modified.

The convergence of the process is measured at iteration $n+1$ by the fluctuation of wake nodes location:

$$\delta(n+1) = \sqrt{\sum_{i=1}^{Nw} [\vec{x}(n+1,i) - \vec{x}(n,i)]^2}\ . \quad (10)$$

Convergence is reached if $\delta(n+1) \approx 10^{-4}\, \delta(1)$. The number of iterations needed ranges between 30 and 80, depending on the test case.

Results presented in this paper are obtained by using 24 x 41 and 90 x 41 panels on each blade and wake respectively (4 wake revolutions) during the iteration process. After convergence the pressure (Cp), thrust (Ct) and torque (Cq) coefficients, etc., are computed again with 38 x 41 panels on the blades to improve the prediction of the torque which is sensitive to the chordwise discretization.

The wake being computed by the potential code, an interface program allows to determine the boundary conditions on nodes of the TASCflow code mesh.

2.2 - Navier-Stokes code (TASCflow)

2.2.1 - Background

In a turbulent flow, quantities such as pressure, velocities, temperature and stresses are time-dependent. These quantities are decomposed into mean and fluctuating components and the original conservation equations are converted to a mean form through a process of time averaging usually called Reynolds-stress averaging, as discussed in [8, 9].

Each dependent variable in these equations is decomposed into a mean component and a fluctuating one. Two decompositions are used, a time-averaged and a mass-averaged techniques (also called Favre averaging). When these decompositions are used, the equations contain terms that cannot be expressed in terms of mean flow variables. These terms are related to known quantities via a turbulence model before a close solution of the equations becomes possible. In the computation presented here the well-known $k-\varepsilon$ turbulence model [10] is used to provide a link between the turbulent transport of momentum and energy and mean flow properties.

The computation of the flow around a rotor is performed in a rotating coordinate system attached to the blades. The formulation of the Reynolds-averaged Navier-Stokes equations in a rotating coordinate system involves additional terms taking into account the effects of Coriolis and centripetal forces.

The relation between the velocity vector C_i in the inertial system, the velocity vector W_i in the rotating system and the rotation velocity vector of the system U_i is as follows (capital letters refer to time-averaged variables):

$$C_i = W_i + U_i \text{ and } U_i = e_{ijk}\,\omega_j\,x_k\,. \tag{11}$$

In this equation the permutation tensor e_{ijk} is used:

$$e_{ijk} = \begin{cases} +1 \text{ for cyclic } ijk, \\ -1 \text{ for acyclic } ijk, \\ 0 \text{ for all other combinations of } ijk. \end{cases} \tag{12}$$

ω_i denotes the vector of rotation system and x_i represents the spatial coordinates in the rotating system.

The equations for the conservation of mass, momentum and energy read respectively:

$$\frac{\partial \rho}{\partial t} + \frac{\partial (\rho W_j)}{\partial x_j} = 0\,, \tag{13}$$

$$\frac{\partial (\rho W_j)}{\partial t} + \frac{\partial (\rho W_j C_i)}{\partial x_j} = -\frac{\partial P}{\partial x_i} - \frac{\partial \left(\tau_{ij} + \rho\,\overline{w_i w_j}\right)}{\partial x_j} - \rho\, e_{ijk}\,\omega_j\,C_k + e_{ijk}\,\omega_j\,x_k \frac{\partial (\rho W_l)}{\partial x_l}, \tag{14}$$

$$\frac{\partial}{\partial t}\left[\rho\left(c_p T + \frac{W_i W_i}{2}\right)\right] - \frac{\partial P}{\partial t} + \frac{\partial}{\partial x_j}\left[\rho W_j\left(c_p T + \frac{W_i W_i}{2} - \frac{\omega_i^2 x_i^2}{2}\right)\right] = \frac{\partial}{\partial x_j}\left(k_{eff}\frac{\partial T}{\partial x_j}\right). \tag{15}$$

In these equations the variables are the time-averaged density ρ, the turbulent fluctuations w_i, the static pressure P and the static temperature T. The overbar refers to the time average of the turbulent variables.

In the momentum equation (14) the viscous stress tensor is given by:

$$\tau_{ij} = -\mu\left(\frac{\partial W_i}{\partial x_j} + \frac{\partial W_j}{\partial x_i}\right), \tag{16}$$

where μ is the molecular viscosity of the fluid. The $k-\varepsilon$ turbulence model expresses the Reynolds stresses as a function of mean deformations:

$$-\rho\,\overline{w_i\,w_j} = \mu_t\left(\frac{\partial W_i}{\partial x_j} + \frac{\partial W_j}{\partial x_i}\right) - \frac{2}{3}\rho\,\delta_{ij}\,k\,, \tag{17}$$

with:

$$\mu_t = \rho\,c_\mu\frac{k^2}{\varepsilon} \text{ and } k = \frac{1}{2}\,\overline{w_i\,w_i}\,. \tag{18}$$

μ_t is the eddy viscosity, k is the turbulent kinetic energy, ε is the dissipation rate of k and c_μ is a constant model.

In the energy equation (15) the enthalpy becomes rothalpy. c_p is the specific heat at constant pressure and $k_{eff} = \lambda + \frac{\mu_t}{Pr_t}c_p$, where λ is the conductivity and Pr_t is the turbulent Prandtl number.

2.2.2 - Grid specification

The computation domain is reduced to a small volume surrounding one rotor blade. This volume consists of a rectangular box where the outer boundary surface, which is parallel to the rotation axis, is cylindrical instead of planar. So the upper and lower surfaces are perpendicular to the rotation axis. The blade geometry is described by taking into account the real blade planform, the real blade sections and the twist. The flight parameters like the pitch, lag and flapping angles are also taken into account in the grid generation.

Many tests have demonstrated that the upstream, downstream, outer and upper boundary surfaces of the domain must be located 2 chords away from the blade. The lower boundary surface is lying 2.5 chords away from the blade. The inner boundary surface is located one chord away from the vertical rotation axis.

These tests have also shown that a minimum of 140 x 24 nodes distributed on the blade is necessary to compute the flow field with enough accuracy. 115 x 40 x 50 nodes are distributed in the whole domain in the chordwise, spanwise and vertical directions, respectively.

2.2.3 - Boundary conditions

The flow field is assumed to be compressible, turbulent and the computation domain rotates with the blade.

Starting from a converged solution of PARSEC, an interface program allows to calculate the velocity vector W_i, the static pressure P and the static temperature T at any point of the flow field. So at every node of the boundary surfaces of the TASCflow grid the previously mentioned quantities are known. It is now sufficient to separate regions where the flow enters and quits the domain of computation: these regions depend on the rotor case.

The velocity vector and the static temperature are assigned at nodes of inlet regions, whereas the static pressure is used for nodes of outlet regions. Having no information about the turbulent aspect of the flow, one specifies that the turbulent kinetic energy k and the dissipation rate ε of k are constant along inlet regions.

2.2.4 - Computation

The TASCflow code is a Finite Volume Method that uses 4 discretization schemes: the Upstream Differencing Scheme (UDS), the Mass Weighted Scheme (MWS), the Linear Profile Scheme (LPS) and a scheme (MLPS) which is intermediate between the last two. The first one is the most robust, whereas the Linear Profile Scheme is the most accurate. A Physical Advection Correction (PAC) may be turned on for each discretization scheme to increase the accuracy of the computation.

A criterion of convergence stops the computation and allows to obtain a stationary converged solution of the problem. This criterion is defined as the maximum current dimensionless residual value for each equation (13) to (15).

A computation is started from an initial guess by using the most robust discretization scheme and a local time step. The first computation is carried out for a hover Mach number of about 0.30.

All computed solutions presented in this paper are converged up to $5 \bullet 10^{-4}$. They are carried out by using the MLPS discretization scheme and the Physical Advection Scheme; the time step corresponds to about 1/120 of the rotation speed.

This code also runs on an IBM RS/6000 workstation; 80 to 120 iterations are needed for a computation starting from an initial guess. When changing the flight conditions, the computation starts from a converged solution and about 15 more iterations are needed to obtain the new converged solution.

3 - Experimental setup

ISL has built a rotor model simulating the hovering flight in order to compare theoretical aspects with measurement. This facility, installed in the open air, is original because the power available at the rotor is such that the rotor head can be equipped with large chord blades. The chord dimension can be from two to four times smaller than that of a full-size helicopter rotor. This apparatus is described in [11 to 13] for details.

The general characteristics of this equipment are as follows:

- maximal power	200 kW,
- power at the rotor head	140 kW,
- maximal speed of the rotor	314 rd/s,
- maximal torque	467 mN,
- height with respect to the ground	2.5 m,
- rotation direction seen from above	clockwise.

The rotor head has a pitching articulation, so that at rest the collective pitch can be changed from 0 to 10° at the blade tip. There is no cyclic pitch as it is not justified in case of hover flight and there is no lagging articulation.

The characteristics of the used blades are as follows:

- rotor diameter	2 m,
- blade root radius	0.28 m,
- type of profile	NACA0012,
- profile chord	0.15 m,
- linear twist	-6.945°/m,
- blade mass	1.4 kg.

The aim of the experiment presented in this paper consists in measuring the components of the aerodynamic force acting on the rotor head, using a six components balance, and the torque driven to the rotor head for many rotation speeds and tip incidence angles.

A shadowgraph arrangement allows to visualize the tip vortices of the rotor blades in order to get the geometrical parameters of the wake. The wake visualization is also performed by using a stroboscopic ombroscopy and a video recording [14]. A Particle Image Velocimetry (PIV) system is used to analyse the tip vortex shed in the wake for many azimuth angles.

4 - Results and discussion

The results obtained with the potential code presented in this paper are carried out with the incompressible version, but the hover Mach number equals 0.6 for the viscous effects calculation. The duration is about 3 minutes and 30 minutes per iteration for PARSEC and TASCflow computations, respectively.

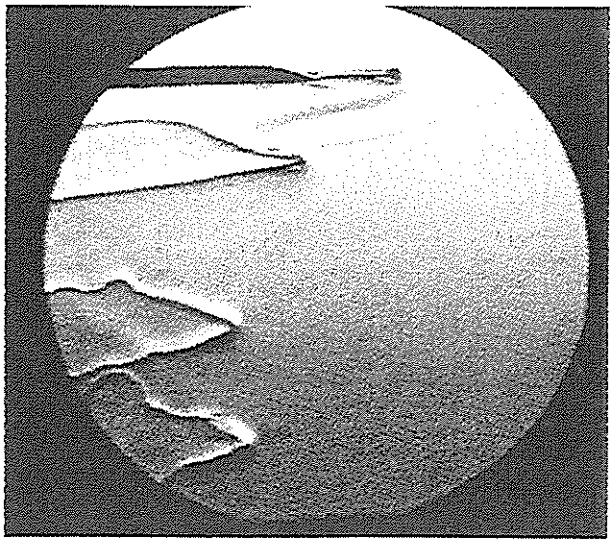

Figure 1: Visualization of the tip vortex shed by a blade; rotation speed: 1500 rev/mn, tip incidence angle: 5°

Figure 1 presents an example of an image recorded for a rotor rotation speed of 1500 rev/mn and a blade tip

incidence angle (θ_{tip}) of 5°. The shadow of 2 interlaced tip vortices (two-bladed rotor) and one blade is reflected by a mirror and can be observed.
Such images allow to get the contraction (r/R) and the convection (z/R) of the tip vortex of one blade versus its age. This has been done for many tip incidence angles and rotation speeds.

Figure 2 depicts the comparison of the measured blade tip vortex path with that computed by the potential code for a rotation speed of 1000 rev/mn and a tip incidence angle of 10°. The tip vortex path is determined by using the shadowgraph and more recently by using the PIV measurement method. Note a good agreement between computation and measurement, especially for the contraction of the wake.

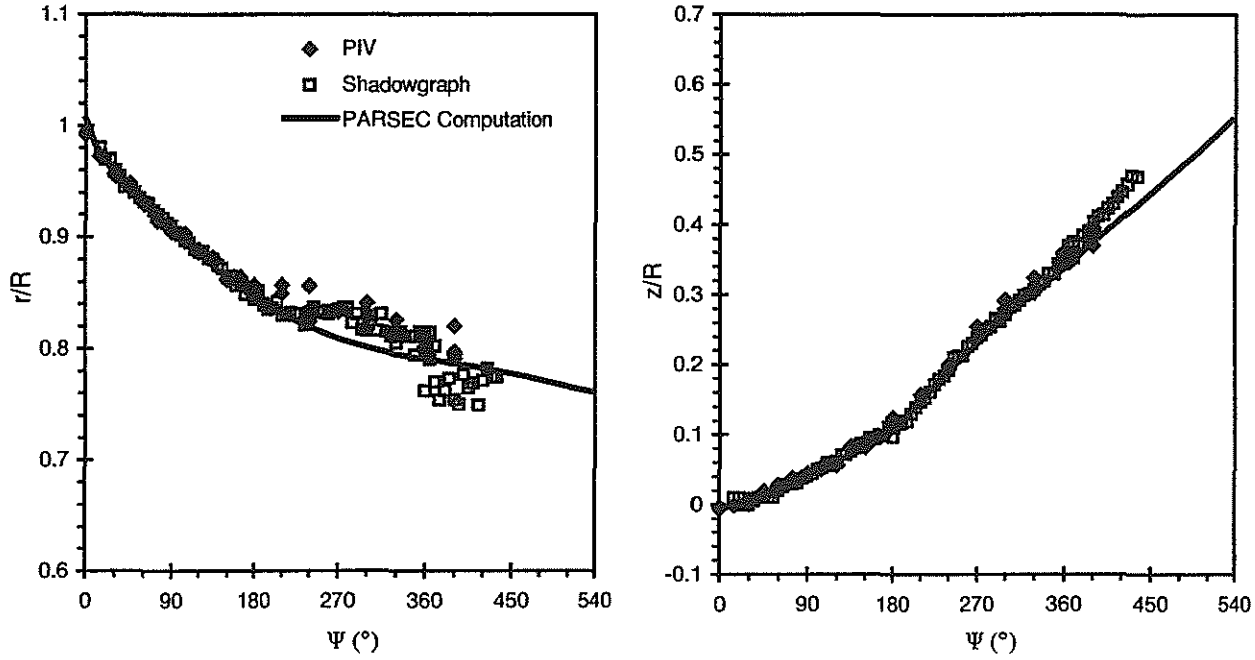

Figure 2: Comparison of the measured tip vortex path with the potential code (r/R: contraction, z/R: convection); rotation speed: 1000 rev/mn, tip incidence angle: 10°

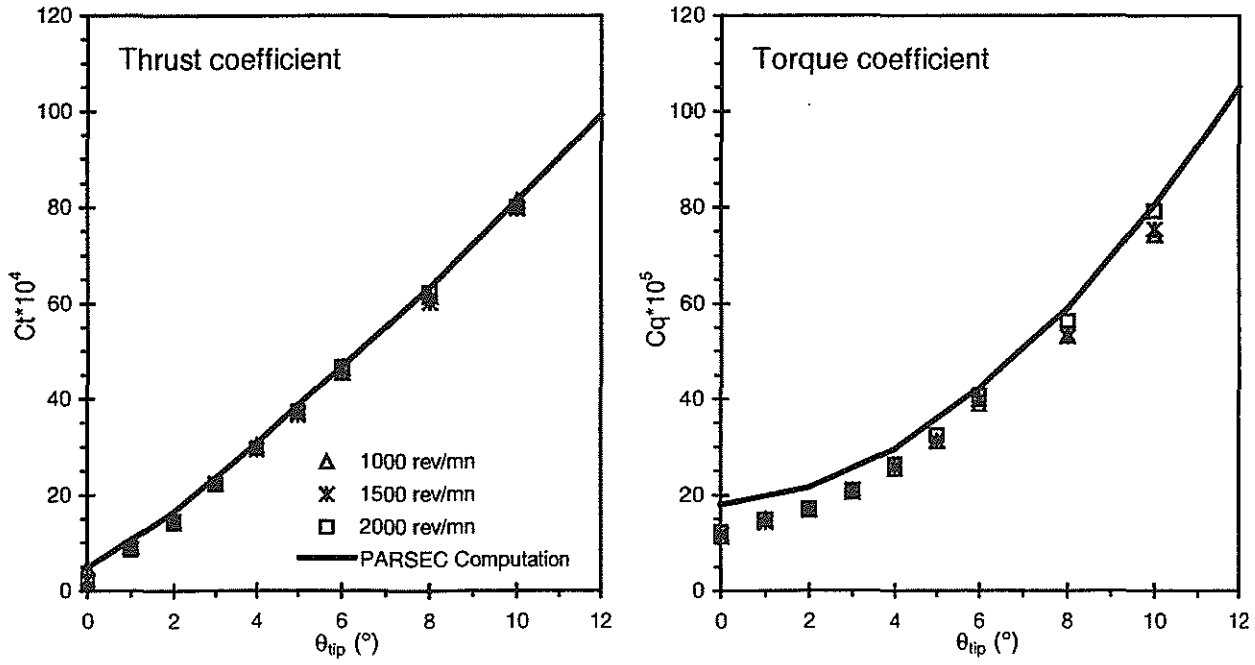

Figure 3: Comparison of measured thrust and torque coefficients with potential code results

Figure 3 shows the comparison of the measured thrust (*Ct*) and torque (*Cq*) coefficients with potential code results for tip incidence angles (θ_{tip}) from 0 to 10° (Mh=0.6). Experimental results are presented for 3 rotation speeds ranging from 1000 to 2000 rev/mn.
A good prediction of the aerodynamic coefficients is found, about 2% on the thrust coefficient, 4 to 12% on the torque coefficient, except for small blade tip incidence angles.

Figure 4 presents the mesh of the boundary surfaces of the TASCflow computation domain, the blade represented by a shaded surface and a grid plane near the blade tip. All TASCflow computations are carried out with this grid; only the blade tip incidence angle changes from one case to the other.

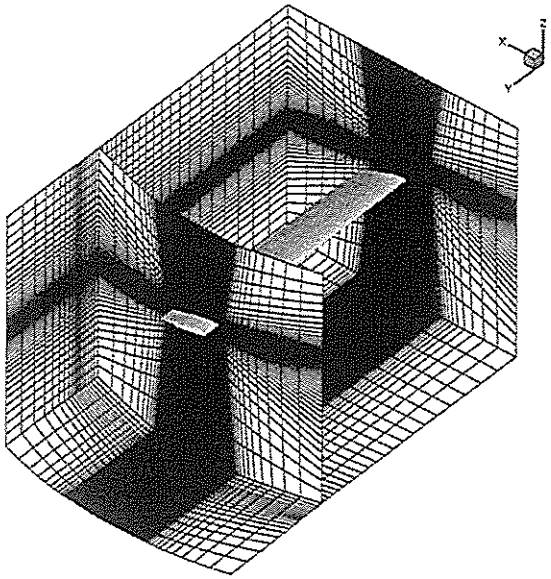

Figure 4: Mesh of the boundary surfaces of the TASCflow computation domain, shaded surface of the blade, grid plane near the blade tip

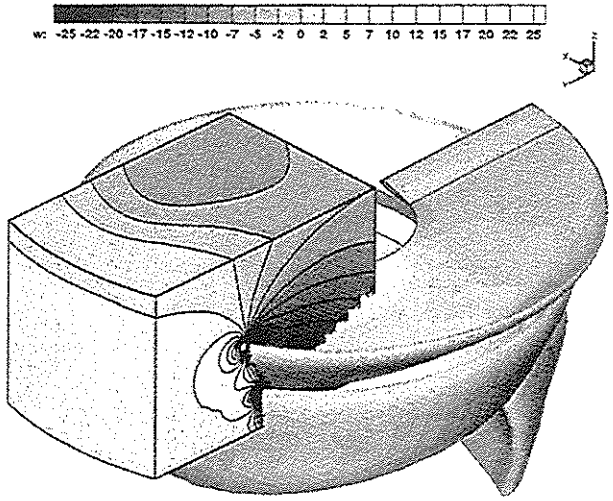

Figure 5: Wake computed by the PARSEC potential code (shaded surface) and axial component of the velocity field on faces of the TASCflow computation domain

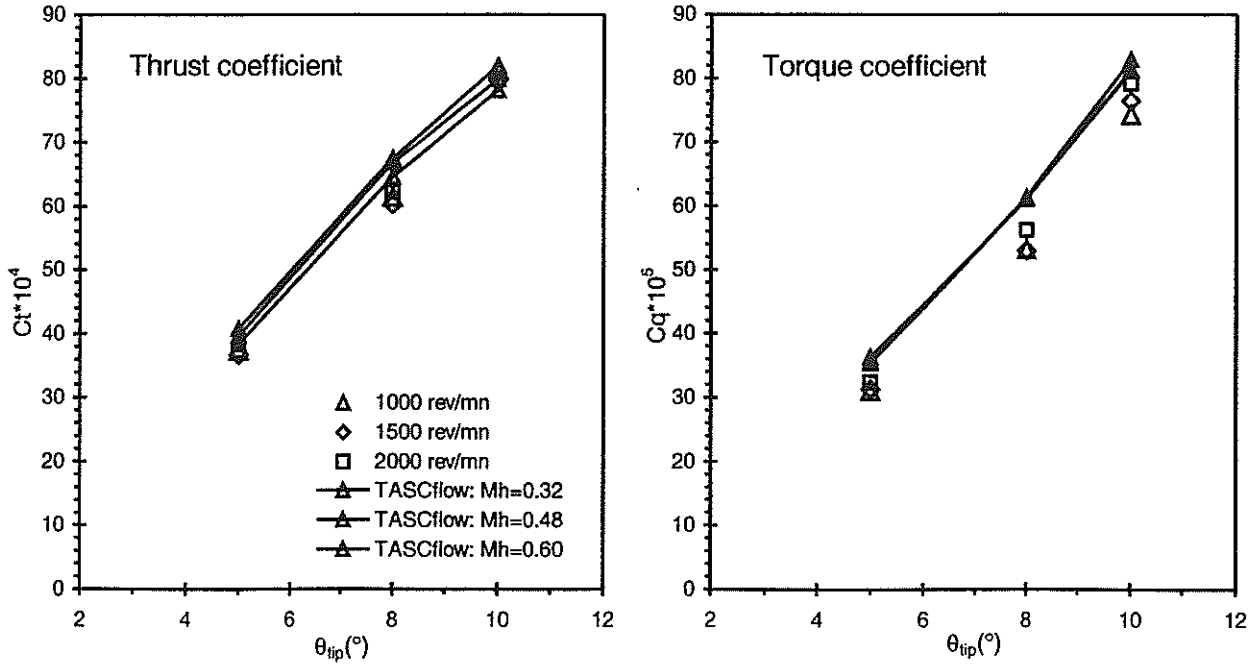

Figure 6: Comparison of measured thrust and torque coefficients with Navier-Stokes code results

Figure 5 depicts an example of rotor blades with the PARSEC computed wakes and the axial component of the velocity field on faces of the TASCflow computation domain (θ_{tip}=10°). Note the rolling-up of the tip vortices and the wake entering the TASCflow domain.

Figure 6 shows the comparison of the measured thrust (*Ct*) and torque (*Cq*) coefficients with TASCflow results for 3 tip incidence angles of 5, 8 and 10°. Computations are carried out for corresponding experimental rotation speeds.
The thrust coefficient is generally overestimated: about 5 to 8% for tip incidence angles of 5 and 8° and only 2% for a 10° tip incidence angle.

The torque coefficient is always overrated by about 15% for hover Mach numbers of 0.32 and 0.48 with tip incidence angles of 5 and 8°. It is overestimated by about 4% for a hover Mach number of 0.60 with a 10° tip incidence angle.
Some 2D experimental and numerical test results supplied by ASC GmbH have shown that the boundary layer near the leading edge region of such an airfoil would be laminar. Unfortunately, the $k-\varepsilon$ turbulence model does not take into account the laminar to turbulent transition of the boundary layer of solid walls.

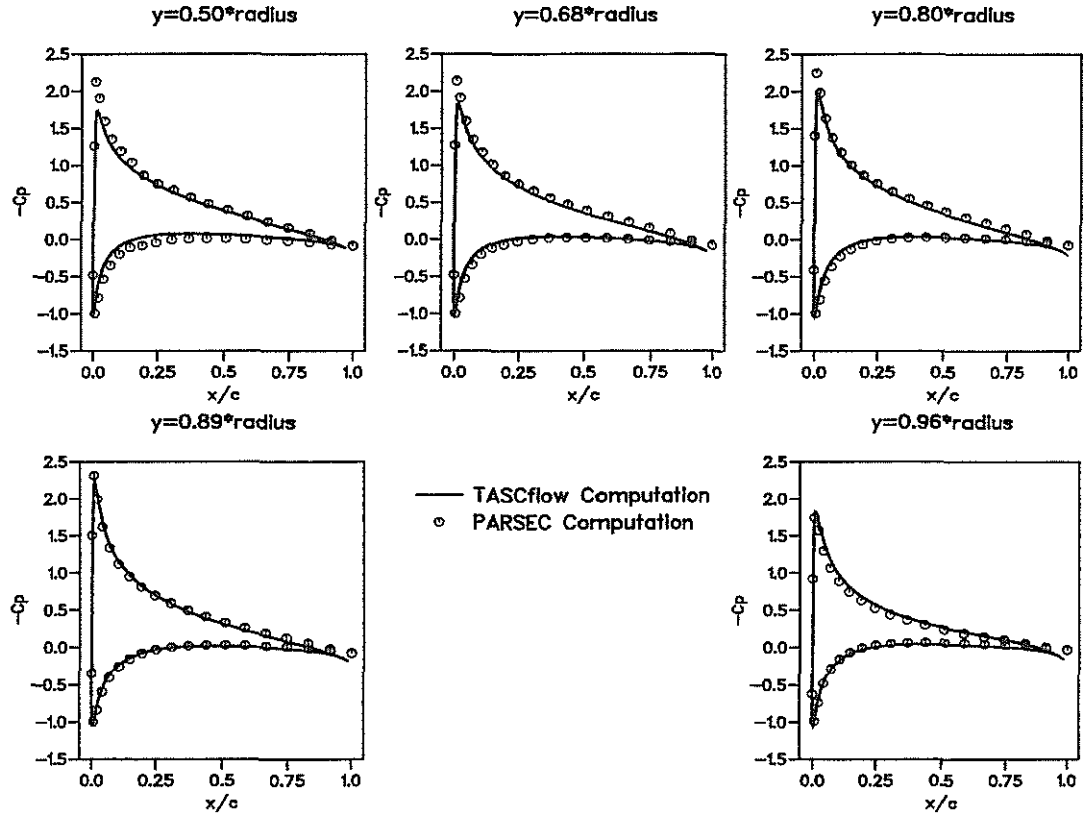

Figure 7: Chord distributions of pressure coefficients computed by PARSEC (Mh=0.60) and TASCflow (Mh=0.32) codes for a 10° tip incidence angle

Figure 7 shows the chord distributions of the pressure coefficients computed by the PARSEC and TASCflow codes for 5 span sections. The tip incidence angle is 10° and the Reynolds number is about $2 \bullet 10^6$; the TASCflow computation is carried out for a hover Mach number of 0.32. Dots, representing the PARSEC results, indicate the location of the chordwise distribution of nodes for that computation.
The main discrepancies concerning computed pressure coefficients appear in the middle of the blade on the leading edge.

Figure 8 presents the same kind of results for a TASCflow hover Mach number of 0.60; PARSEC results remain the same as for figure 7.
When comparing with figure 7, one notes the increase of the pressure coefficient on the leading edge near the blade tip where the supersonic zone appears.

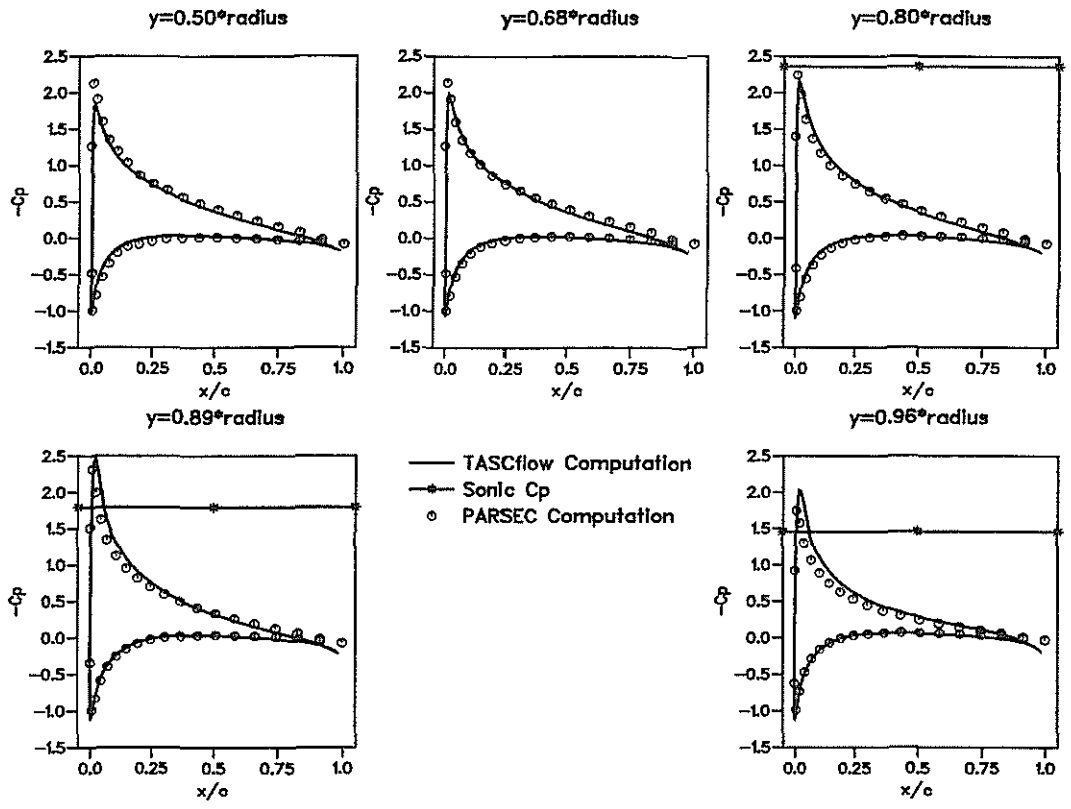

Figure 8: Chord distributions of pressure coefficients computed by PARSEC (Mh=0.60) and TASCflow (Mh=0.60) codes for a 10° tip incidence angle

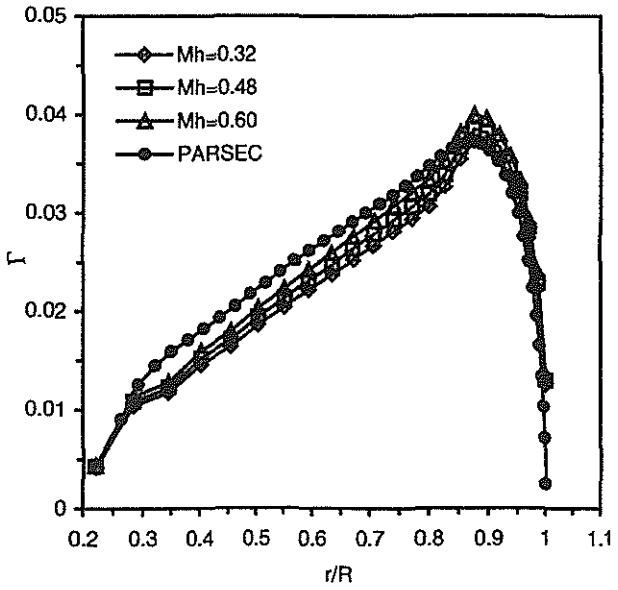

Figure 9: Spanwise distribution of the normalized circulation ($\frac{\Gamma}{\Omega R^2}$) computed by PARSEC and by TASCflow (Mh=0.32 to 0.60) codes for a 10° tip incidence angle

Figure 9 shows the comparison of the spanwise distribution of the computed normalized circulation obtained with PARSEC and TASCflow (Mh=0.32 to 0.60) for a tip incidence angle of 10°. Markers indicate the spanwise distribution of nodes for these computations. Discrepancies between PARSEC and TASCflow are most important from the blade root to 0.8 radius. The maximum of circulation obtained by PARSEC corresponds to that of TASCflow for a hover Mach number of 0.32. These results are coherent with those of figures 7 and 8.
The circulation computed by TASCflow increases with the hover Mach number.

5 - Conclusion

The panel method and the free-wake calculation presented in this paper give reliable results without needing any trimming empirical data. A good correlation with the experimental data from the ISL rotor model is found concerning the thrust and torque coefficients and the wake geometry.

Our original approach consisting in coupling this panel method with a Navier-Stokes method allows to mesh only the near volume surrounding one blade instead of the whole volume around the rotor. A good prediction of the

thrust coefficient is found, but a slight overestimate of the torque is obtained. These results would probably be improved by taking into account the laminar to turbulent transition of the boundary layer of the blade.

The investigation of the aerodynamic performances on advanced blades can now be regarded as the final goal of this study. As an example, figure 10 shows the comparison of the measured figure of merit (*Fm*) versus *Zbar* with PARSEC and TASCflow computations for a EUROCOPTER rotor with a swept and anhedral blade tip. The predictions are very encouraging; however, TASCflow results will probably be improved when a transition model from laminar to turbulent boundary layer is available.

This approach also has the great advantage of running on a low-cost workstation with an acceptable computation duration consistent with the specifications of helicopter manufacturers.

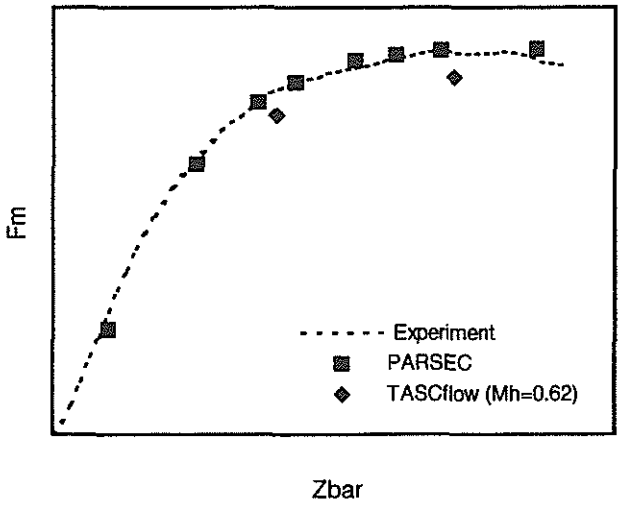

Figure 10: Comparison of measured figure of merit ($Fm = \frac{\sqrt{0.5\,Ct^3}}{Cq}$) versus *Zbar* ($Zbar = \frac{200\,Ct}{\sigma}$, σ =solidity) with numerical results for an advanced EUROCOPTER rotor

Acknowledgements

The authors thank G. Arnaud and F. Toulmay from EUROCOPTER for useful discussions and suggestions.

Bibliography

[1] F. Farassat, M.K. Myers, "Extension of the Kirchhoff's Formula to Radiation from Moving Surfaces", Journal of Sound and Vibration, 123(3), 451-460, 1988

[2] L. Morino, M. Gennaretti, U. Iemma, F. Mastroddi, "A General Boundary Element Method for Aerodynamics and Aeroacoustics of Rotors", in 18th European Rotorcraft Forum, Avignon, September 15-18, 1992

[3] P. Baude, "Etude des écoulements transsoniques à l'aide de la méthode des panneaux. Application au rotor d'hélicoptère en vol stationnaire", Doctorate thesis, ISL report - R 105/97, 1997

[4] J. Haertig, M. Schaffar, P. Gnemmi, "Rotor Loads Computation Using Singularity Methods and Application to the Noise Production", in 17th Congress of the International Council of the Aeronautical Sciences, Stockholm, Sweden, September 9-14, 1990

[5] D.E. Hoak, "USAF Stability and Control DATCOM", McDonnell-Douglas Corporation, October 1960, revised January 1975, Berlin, 1972

[6] J. Bousquet, "Méthode des singularités", Cepadues Editions, Toulouse, 1990

[7] R.I. Lewis, "Vortex Element Methods for Fluid Dynamic Analysis of Engineering Systems", Cambridge University Press, 1991

[8] T. Cebeci, A.M.O. Smith, "Analysis of Turbulent Boundary Layers", Academic Press, Inc., New-York, USA, 1974

[9] Advanced Scientific Computing Ltd, "TASCflow, Theory Documentation"

[10] B.E. Launder, D.B. Spalding, "The Numerical Computation of Turbulent Flows", Comp. Meth. Appl. Mech. Eng., Vol. 3, pp. 269-289, 1974

[11] P. Gnemmi, J. Haertig, Ch. Johé, "Validation of the ROTAC Code for the Rotor Noise Prediction", in 18th European Rotorcraft Forum, Avignon, France, September 15-18, 1992

[12] P. Gnemmi, "Contribution à la prévision du bruit rayonné par un rotor d'hélicoptère en régime subsonique", Doctorate thesis, ISL report - R 108/93, 1993

[13] P. Gnemmi, J. Haertig, Ch. Johé, F. Albe, "Measurements on the ISL Rotor Model", in 15th International Congress on Instrumentation in Aerospace Simulation Facilities (ICIASF'93)
ISL, Saint-Louis, France, June 2-5, 1992, ISL report - CO 220/92

[14] J. Haertig, F. Albe, Ch. Johé, "Visualisation par ombroscopie du sillage des pales du rotor ISL", in 6ème Colloque National de Visualisation et de Traitement d'Images en Mécanique des Fluides, Saint-Etienne, France, May 30 - June 2, 1995